NANO LETTERS
Cite This: Nano Lett. XXXX, XXX, XXX−XXX
Letter
pubs.acs.org/NanoLett

Near-Field Electrospinning for Three-Dimensional Stacked Nanoarchitectures with High Aspect Ratios

Yang-Seok Park,[†,‡,⊥] Junyoung Kim,[†,‡,⊥] Jung Min Oh,[†,‡,∥] Seungyoung Park,[§] Seungse Cho,[§] Hyunhyub Ko,[§] and Yoon-Kyoung Cho*[,†,‡,§]

[†]Department of Biomedical Engineering, School of Life Sciences, Ulsan National Institute of Science and Technology (UNIST), Ulsan 44919, Republic of Korea

[‡]Center for Soft and Living Matter, Institute for Basic Science (IBS), Ulsan 44919, Republic of Korea

[§]School of Energy and Chemical Engineering, Ulsan National Institute of Science and Technology (UNIST), Ulsan 44919, Republic of Korea

Supporting Information

ABSTRACT: Near-field electrospinning (NFES) was developed to overcome the intrinsic instability of traditional electrospinning processes and to facilitate the controllable deposition of nanofibers under a reduced electric field. This technique offers a straightforward and versatile method for the precision patterning of two-dimensional (2D) nanofibers. However, three-dimensional (3D) stacked structures built by NFES have been limited to either micron-scale sizes or special shapes. Herein, we report on a direct-write 3D NFES technique to construct self-aligned, template-free, 3D stacked nanoarchitectures by simply adding salt to the polymer solution. Numerical simulations suggested that the electric field could be tuned to achieve self-aligned nanofibers by adjusting the conductivity of the polymer solution. This was confirmed experimentally by using poly(ethylene oxide) (PEO) solutions containing 0.1−1.0 wt% NaCl. Using 0.1 wt% NaCl, nanowalls with a maximum of 80 layers could be built with a width of 92 ± 3 nm, height of 6.6 ± 0.1 μm, and aspect ratio (height/width) of 72. We demonstrate the 3D printing of nanoskyscrapers with various designs, such as curved "nanowall arrays", nano "jungle gyms," and "nanobridges". Further, we present an application of the 3D stacked nanofiber arrays by preparing transparent and flexible polydimethylsiloxane films embedded with Ag-sputtered nanowalls as 3D nanoelectrodes. The conductivity of the nanoelectrodes can be precisely tuned by adjusting the number of 3D printed layers, without sacrificing transmittance (98.5%). The current NFES approach provides a simple, reliable route to build 3D stacked nanoarchitectures with high-aspect ratios for potential application in smart materials, energy devices, and biomedical applications.

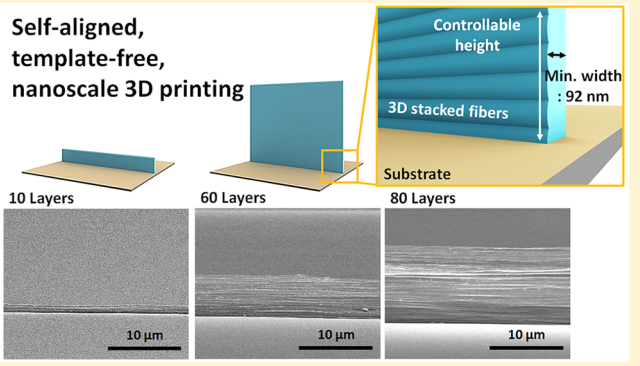

KEYWORDS: *Nanofiber, near-field electrospinning, multilayer, transparent electrode, 3D printing*

Electrospinning is a well-established technique for the fabrication of various types of nanofibers with different compositions and structures. Electrospun nanofibers have been used for a broad range of applications, including filtration membranes, catalysts, electronic devices, and biomedical scaffolds.[1] However, the uncontrollable nature of the electrospun jet limits the application of this technique to the fabrication of devices that do not require precisely deposited fibers.[1] In contrast, controlled nanofiber deposition can be realized by near-field electrospinning (NFES), as the bending instability of the jet is significantly reduced because the distance between the nozzle and the collector is reduced to a few centimeters (typically <5 cm), and the applied voltage is lowered to several hundred volts.[2,3] Furthermore, the collector can be moved in the $X-Y$ direction at a programmable speed, allowing various micro/nanopatterns of waved or straight fibers to be prepared.[3−8]

Although NFES has various advantages, such as low-voltage deposition, precise patterning of fibers, minimum consumption of materials, and good position controllability, its use is typically limited to creating two-dimensional (2D) structures on flat surfaces.[9] Nevertheless, three-dimensional (3D) mesh structures can be built[10−15] by layer-by-layer additive printing by NFES using highly viscous polymer melts, as they have improved directional stability toward the grounded collector in comparison to the polymer solutions used in conventional electrospinning and NFES processes. For example, Wunner et

Received: October 9, 2019
Revised: November 22, 2019
Published: November 25, 2019

DOI: 10.1021/acs.nanolett.9b04162
Nano Lett. XXXX, XXX, XXX−XXX

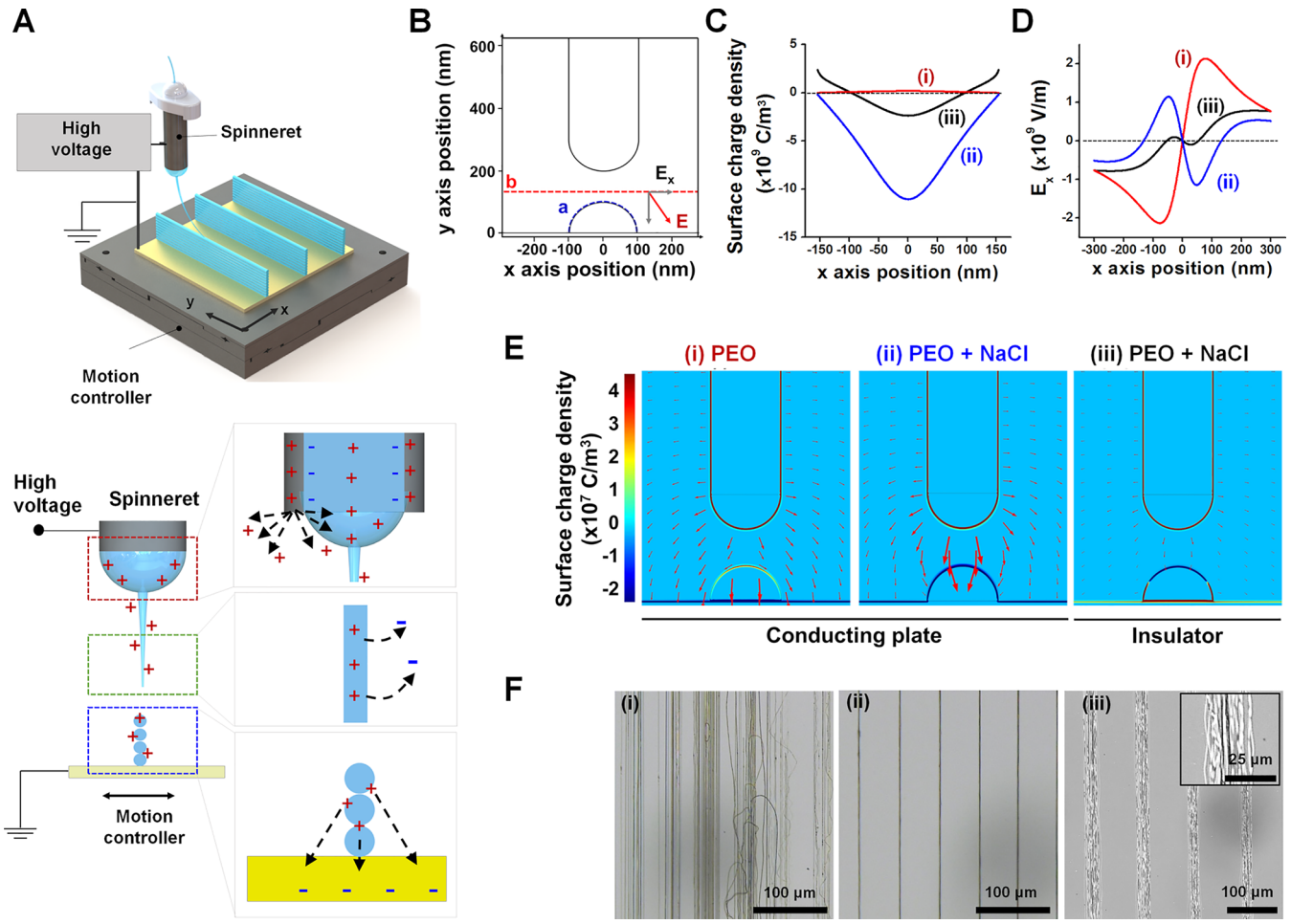

Figure 1. High-resolution near-field electrospinning (NFES) 3D nanoprinting for the fabrication of 3D nanofibrous structures. (A) Schematic presentation of the experimental setup. Charge carriers are generated in the polymer solution via charge emission with a conducting spinneret, followed by charge dissociation from the bulk liquid during the flight phase and after deposition on the collecting electrode, based on surface contact and inverse corona discharges. (B) Two-dimensional schematic diagram depicting the geometry used in the numerical simulation. (C) Surface charge density at surface "a" and (D) *x*-component of the electric field strength along line "b" for the three cases in (E); field focusing is observed for case (ii). (E) Simulation results for printing (i) pure poly(ethylene oxide) (PEO) solution and (ii) PEO + NaCl solution on a conducting plate, and (iii) PEO + NaCl solution on an insulating surface. Electric field arrows and surface charge density contours are shown. (F) Optical images of the 3D printed nanofibers corresponding to the three cases in (E). (i) Pure PEO solution on a conductive plate: no 3D stacking owing to repulsion between the electrospun jet and the deposited fibers due to their high residual charge. (ii) PEO + NaCl solution on a conductive plate: considerably higher precision nanofiber alignment and stacking owing to the negative charge of the deposited fibers. (iii) PEO + NaCl solution on insulating material: misaligned stacked nanofibers owing to the partial negative charge on the as deposited fibers due to reduced charge dissipation.

al. demonstrated[14] the fabrication of thick scaffold structures from micrometer-sized fibers using multilayer additive printing with a highly viscous polymer melt. To promote accurate alignment in the vertical direction, they adjusted the distance between the spinneret and the collector and increased the applied voltage to compensate for electric repulsion between the deposited polymer and successive fibers. However, highly viscous polymer melts typically produce much thicker fibers (on the order of several micrometers) than those obtained via conventional far-field electrospinning or solution-based NFES processes.[16,17]

It has been demonstrated[18] that nanoscale 3D structures can be fabricated by the repetitive deposition of nanofibers onto a metal electrode on an insulating collector. However, patterning of the conducting electrode is a prerequisite, as the shapes of the nanowalls are dictated by the predesigned pattern on the electrode.[18] Kim et al. reported[19] a hollow pottery structure constructed by the spontaneous coiling of electrospun nanofibers when a sharp electrode tip was positioned underneath an insulating substrate. However, the constructed structures were limited to hollow cylindrical shapes. Zhao et al. demonstrated[20] that the patterns of electrospun fiber mats could replicate topographical features such as protrusions on the insulating substrate. It was shown that the insulating substrate could be polarized upon the application of a strong external electric field that could affect the distribution of the intrinsic electric field. Furthermore, adsorbed water molecules[21] or functional electrolyte patterns[22] on insulating substrates or electrolyte solutions[23] could serve as conducting collector electrodes that allow the deposition of electrospun fibers. Luo et al.[24] used printing paper as a collecting substrate, whereby the residual solvent from the deposited fibers could wet the paper and thus connect to the grounded plate. The fibers were selectively attracted on top of the previously deposited fibers to form 3D architectures. However, this process required a wicking substrate, and the diameters of the

DOI: 10.1021/acs.nanolett.9b04162
Nano Lett. XXXX, XXX, XXX−XXX

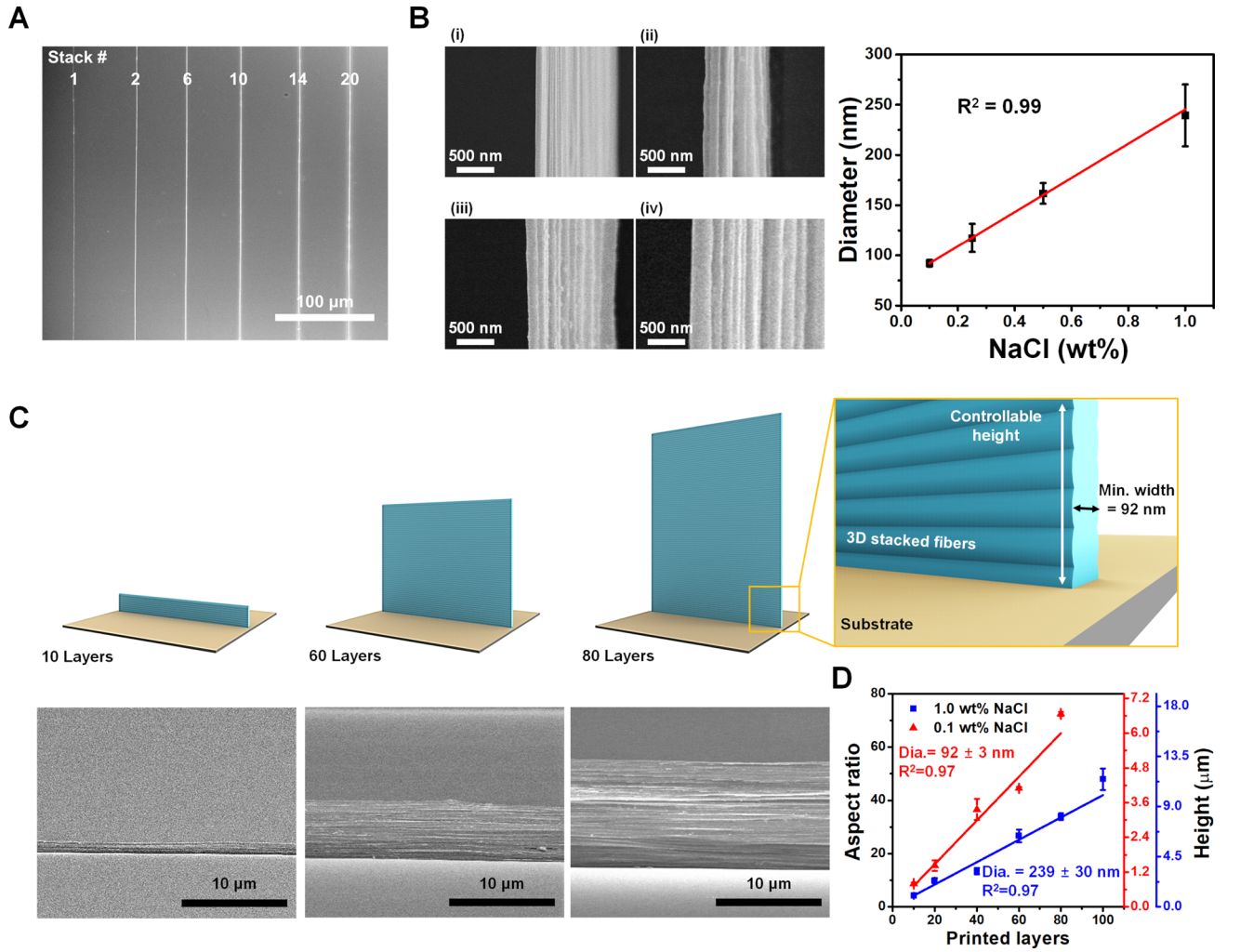

Figure 2. Precise printing control of 3D nanofibrous structures. (A) SEM image (top view) of constructed nanowalls with different numbers of layers. (B) Nanowall diameter depending on the NaCl concentration of the PEO solution: (i) 0.1 wt% (92 ± 3 nm), (ii) 0.25 wt% (117 ± 14 nm), (iii) 0.5 wt% (161 ± 10 nm), and (iv) 1 wt% (239 ± 30 nm). (v) Linear relationship between the NaCl concentration and the fiber diameter (R^2 = 0.99). (C) Schematic and SEM images (side views) of 3D printed nanowalls consisting of different numbers of nanofiber layers. (D) Linear relationship between the nanowall height and the number of stacked layers (R^2 = 0.97).

fibers were relatively large (on the order of several micrometers). In summary, to the best of our knowledge, self-aligned and stacked 3D structures built via layer-by-layer printing by design using NFES have been limited to the micron scale or to specific prefabricated shapes, such as hollow cylinders or nanowalls, based on specific collector requirements. Despite the importance of low-cost, versatile, and reliable methods for the controlled alignment and patterning of 3D nanostructures with high precision, the currently available methods are rudimentary.

Herein, we introduce a precise direct-write 3D nanoprinting process based on NFES that can build template-free, self-aligned, 3D stacked, and high aspect ratio nanostructures without any prior requirements for the collector design. By simply adding salt to the PEO solution, we could ensure precision patterning and self-alignment in the *Z*-axis with precise control of the layer-by-layer nanofiber deposition. Using this modification, we were able to print nanowalls with thicknesses of 92 ± 3 to 239 ± 30 nm and aspect ratios (height/width) of 48−72 depending on the concentration of salt in the PEO solution. Various 3D nanoarchitectures were designed and created, such as curved nanowalls, nano jungle gyms, and nanobridges. We then elucidated the fundamental mechanism that enabled the spontaneous self-stacking of nanofibers on top of each layer and demonstrated the applicability of this technique in the field of nanoelectronics by using the 3D printed nanowalls as templates to pattern transparent nanoelectrodes with controllable electrical resistances.

The modified NFES process provided high-resolution control of the width and height of the self-stacked nanowalls (see Figure 1). NFES enables the precise deposition of a stable jet by accurately positioning the spinneret tip a short distance from the collector. Straight nanofibers can be printed by moving the substrate faster than the electrospinning deposition rate. Here, we 3D printed multiple layers of nanofibers by moving the motorized stage back and forth in the *Y*-direction (at a fixed *X*- and *Z*-position).

During conventional electrospinning, a high voltage is applied to the needle of the syringe that contains the polymer solution, and this voltage is grounded to the collector substrate. As extensively reviewed by Collin et al.,[25] the generation of charge carriers in the polymer solution is primarily determined by two processes: the direct injection of charge carriers into

DOI: 10.1021/acs.nanolett.9b04162
Nano Lett. XXXX, XXX, XXX−XXX

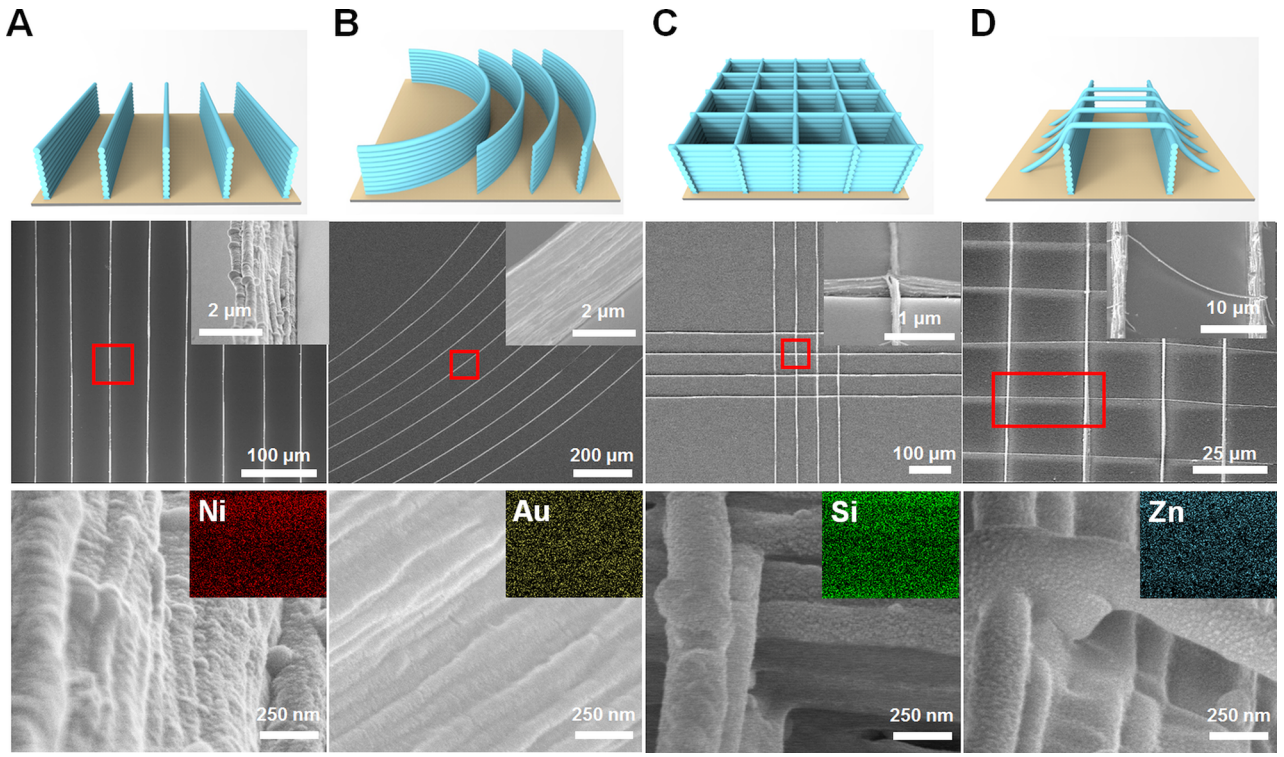

Figure 3. Schematics, SEM images, and EDS maps of various 3D printed nanoarchitectures coated with different functional materials (Ni, Au, SiO_2, and ZnO). (A) Straight Ni nanowalls comprising 40 nanofiber layers (distance between walls: 50 μm). (B) Curved Au nanowalls comprising 40 nanofiber layers (distance between walls: 100 μm). (C) SiO_2 grid pattern comprising 40-layer high nanowalls (distance between walls: 50 μm). (D) ZnO nanobridges comprising 40-layer high nanowalls (distance between walls: 25 μm) connected by single fibers suspended between the nanowalls (distance between suspended fibers: 25 μm). All fibers were fabricated under the same NFES conditions (described in Experimental Methods in SI) with different G-codes for the stage movement.

the liquid from conducting materials under strong electric fields and charge dissociation from dissolved ion pairs that already exist in the bulk of the liquid. These mechanisms provide excess charge carriers to the polymer solution, which accelerates the force of the jet toward a grounded collector. The charge dissipates both in the flight phase and after deposition on the collecting electrode. The charge dissipation mechanisms are two-fold, including a surface contact discharge and an inverse corona discharge from the deposited fiber to the conducting substrate. However, the charge does not fully dissipate, leaving the solidified fibers with a considerable residual charge (Figure 1A). As the charged fibers accumulate on the collecting substrate, the electric field is screened. Although the physical mechanism of charge generation in electrospun fibers is fairly well understood, the charge dissipation mechanism of solidified fibers has not been fully elucidated.[25]

We hypothesized that by enhancing the charge dissipation through the collecting substrate, the electric field could be focused toward the predeposited nanofiber, which would optimize the electrospinning conditions. Moreover, an accelerated discharge process should enhance the self-stacking and precision of 3D printed nanofibers. We performed finite element analyses with COMSOL Multiphysics to identify the electric fields guiding the electrospun jets when using conductive or nonconductive polymer solutions and substrates, as shown in Figure 1B–E. When pure PEO solution (nonconductive) was deposited on a conducting substrate (Figure 1E(i)), the deposited fibers had a weak positive surface charge. Moreover, the x-component of the electric field guiding the fiber deposition was in the repulsive direction. On the other hand, as the conductivity of the polymer solution was increased by adding NaCl (Figure 1E(ii)), the surface charge density of the deposited fibers became negative; this created an attraction between the nanofiber stream and the previously deposited fibers. The charge dissipation was less efficient when using an insulating substrate (Figure 1E(iii)), which reduced the negative surface charge density and the degree of focusing. The detailed physical parameters used in the simulation are given in the Supporting Information (Tables S1 and S2).

These theoretical predictions were confirmed experimentally by 3D printing nanofibers under the same conditions. When pure PEO solution was printed, the nanofibers were deposited in random X positions (Figure 1F(i)), probably because of the repulsive force generated between the nanofiber jet and the previously deposited fibers. Conversely, when the PEO solution contained a small amount of NaCl (0.1–1.0 wt%), 3D stacked self-aligned nanofibers were synthesized (Figure 1F(ii)). We expect that this self-stacking phenomenon results from the efficient charge dissipation from the deposited fiber. To confirm this hypothesis, we used an insulating substrate as the grounded collector (e.g., SiO_2 film on a silicon wafer); it was observed that the precision of the self-alignment was diminished (Figure 1F(iii)). However, precise self-aligned 3D printed nanoarchitectures were obtained when using various conducting substrate, including doped Si, Au, and ITO (Figure S1). This observation implies that charge dissipation from the deposited fibers is crucial for inducing an electrical force to accurately guide the nanofiber jet. Efficient charge dissipation dramatically increases the surface polarization, which in turn

DOI: 10.1021/acs.nanolett.9b04162
Nano Lett. XXXX, XXX, XXX–XXX

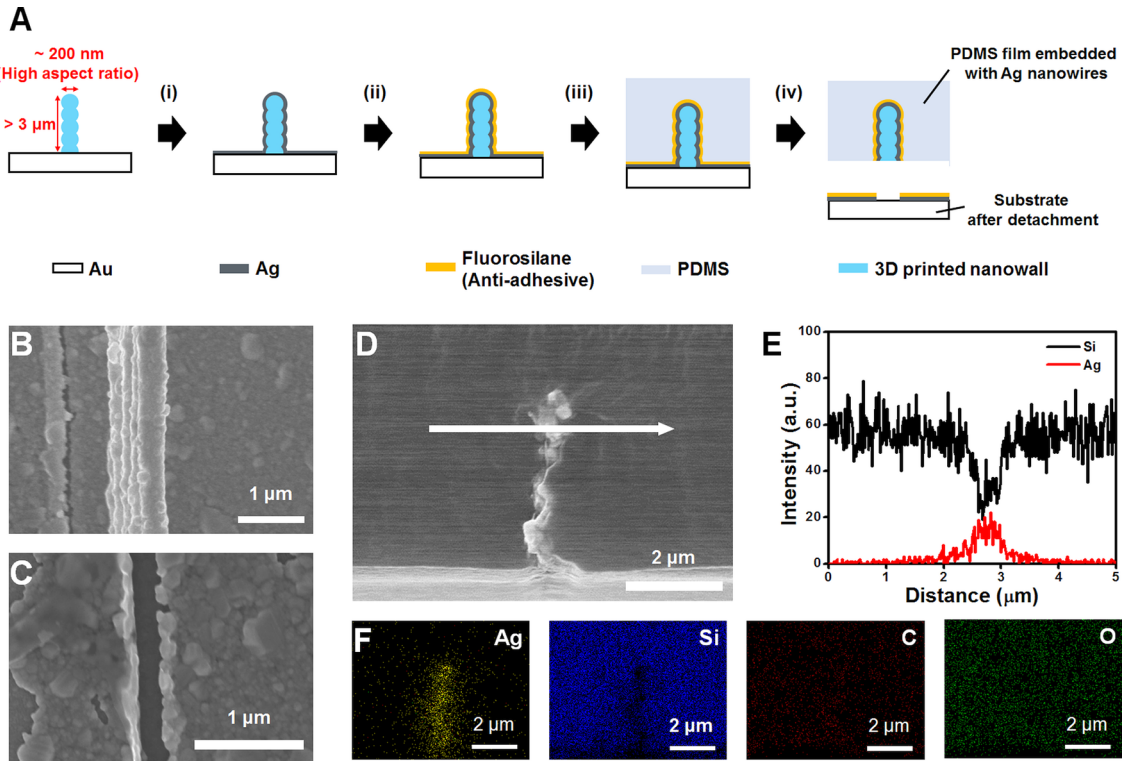

Figure 4. Fabrication of transparent electrodes embedded with 3D Ag nanowire architectures using 3D printed nanofibers. (A) Scheme showing the fabrication of a conductive polydimethylsiloxane (PDMS) film embedded with Ag nanowires: (i) Ag sputtering, (ii) anti-adhesive coating, (iii) PDMS coating, and (iv) detachment. (B–D) SEM images of the transfer process: (B) top view of the PDMS film embedded with Ag nanowires, (C) top view of the substrate after the transfer of Ag nanowires, and (D) cross-sectional view of the PDMS film embedded with Ag nanowires. SEM–EDS (E) line scan and (F) elemental mapping of the PDMS film embedded with 3D Ag nanowires.

induces a higher attraction between the nanofiber jet and the deposited fiber.

The attraction between the nanofiber jet and deposited polymer was stronger at higher salt concentrations (i.e., at higher conductivities), even when the substrate was stationary (Figure S2 and Video S1). However, when pure PEO solution was used, the repulsive force accumulated after the fibers were deposited in a particular area, causing the jet to move to a new location. With a more conductive polymer solution, when we applied an electric field, the previously deposited fiber was strongly attracted to the Taylor cone (Video S2). This strong attraction was not observed when the voltage was turned off, or when the polymer solution did not contain salt (Video S2), which suggests that the deposited nanofibers were negatively charged when using PEO salt solution.

We were able to construct 3D nanoarchitectures with controllable dimensions by manipulating the motion of the stage during 3D NFES to deposit the nanofibers in desired patterns, as shown in Figures 2 and S3. For example, nanowalls of a desired height could be built by stacking a precise number of nanofiber layers (R^2 = 0.97; Figure 2C, D). The scanning electron microscopy (SEM) images in Figure 2C show side views of 3D nanowalls with different numbers of layers. The orderly morphology of the stacked nanolayers can be seen in detail. With a 1 wt% NaCl PEO solution, we successfully produced nanowalls comprising up to 100 nanofiber layers (height, 1.0 ± 0.2 to 11.4 ± 0.9 μm; mean thickness, 239 ± 30 nm; length, 2 cm; maximum aspect ratio (height/width), 48). The width of the 3D nanoarchitecture decreased linearly as the salt concentration decreased (Figure 2B), reaching 92 ± 3 nm at 0.1 wt% NaCl (height, 0.8 ± 0.1 to 6.6 ± 0.1 μm; maximum aspect ratio, 72). However, at higher NaCl concentrations (2.0 wt%), the width of the fiber was not uniform and the surface was rough; at lower concentrations (<0.1 wt%), we could not achieve precise self-stacking. Therefore, the optimized experimental condition uses PEO solution with 0.1–1 wt% NaCl.

The self-assembly of 3D fibrous structures has been reported previously[26−29] in conventional far-field electrospinning on account of electrostatic forces between the previously deposited material and the aerial fibers. However, the electrospun fibers were either formed into irregular 3D spongiform fiber stacks[26,27] or peculiar honeycomb-shaped foamlike structures.[28,29] Here, the proposed 3D nanoprinting technique could create various "nanoskyscraper" designs using preprogrammed X–Y stage motion. Once built, the 3D printed polymer nanoarchitectures could be stably coated with functional materials (e.g., Ni, Au, SiO_2, and ZnO). To demonstrate the versatility of this process, we produced straight Ni nanowall arrays, curved Au nanowall arrays, and SiO_2 nanojungle gyms from 40-layer high nanowalls (mean height, 3.2 ± 0.3 μm; mean thickness, 239 ± 30 nm) and produced ZnO nanobridges by suspending single fibers on top of two such nanowalls. The structures were analyzed by SEM and energy dispersive X-ray spectroscopy (EDS), as shown in Figures 3 and S5. When 1.0 wt% NaCl PEO solution was used, the 3D nanowalls could be built at a distance of 25–100 μm from each other (Figure S4). When the pitch was less than 25 μm, the stacked fibers were misaligned owing to electrostatic interference from the nearby 3D structures.

To demonstrate a potential application of the nanoarchitectures built by the proposed NFES method, nanowalls

DOI: 10.1021/acs.nanolett.9b04162
Nano Lett. XXXX, XXX, XXX–XXX

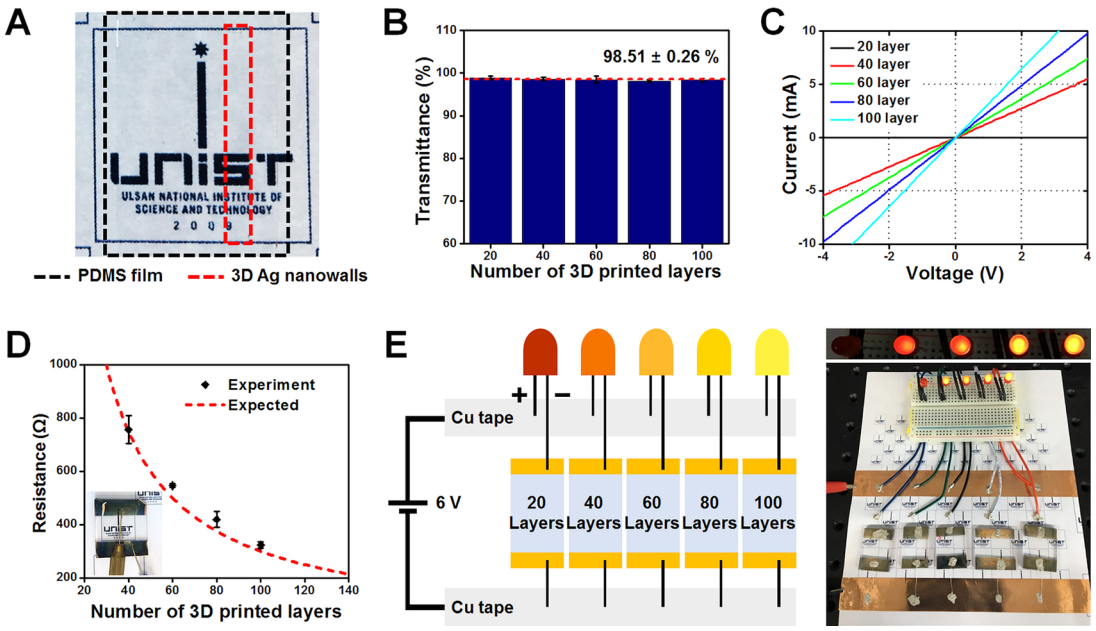

Figure 5. Optical and electrical characterization of transparent electrodes. (A) Optical image of transparent PDMS electrode with embedded 3D Ag nanowires. (B) Transmittance of the transparent electrodes depending on the number of 3D printed layers of Ag nanowires (20−100 layers). The average transmittance was 98.5%. (Note that this does not include the transmittance of the substrate.) (C) Current−voltage (I−V) curve of PDMS transparent electrodes embedded with multilayered 3D Ag nanowires (20−100 layers). All electrodes yielded stable ohmic contacts. (D) Experimental and expected resistances of the transparent electrodes with 40−100-layer high embedded Ag nanowires. (E) Setup to identify the resistance tunability of the transparent electrodes based on an LED intensity comparison. Permission received for use of logo in panels A,D, and E.

with high aspect ratios were sputtered with Ag and used as a template to prepare transparent and flexible PDMS substrates embedded with 3D nanoelectrodes. As shown in Figure 4A, the 3D nanowall arrays were initially sputtered with Ag (100 nm), followed by the deposition of an antiadhesive coating. After PDMS casting, the PDMS film and embedded 3D Ag nanowires were gently detached from the substrate. The antiadhesive coating played an important role in separating the PDMS layer from the substrate. The presence of Ag nanowires with a width of 400 nm and height of 3.3 ± 0.3 μm embedded in the PDMS film was further confirmed by SEM−EDS analyses (Figures 4B−F and S6).

The optical and electrical properties of the 3D Ag nanowire-embedded PDMS film were then characterized. As shown in Figure 5A, the electrode is highly transparent; the "UNIST" letters are clearly visible through the film. The transmittance in the visible wavelength was maintained at ∼ 98.5% (Figure 5B). Moreover, irrespective of the wavelength, high-transmittance values (98−99%) were attained for transparent electrodes with embedded 3D Ag nanowires of different heights (Figure S7). To analyze the electrical properties, transparent electrodes were prepared using arrays of ten 3D printed nanowires of various heights (20−100 layers) and a pitch of 50 μm. The current−voltage (I−V) curves of the transparent electrodes (Figure 5C), obtained under direct current (DC) voltage sweeping mode from −4 to 4 V, yielded a stable ohmic contact. The electrical resistance, sheet resistance, and resistivity were estimated from the measurements and are listed in Table S3. As shown in Figure 5D, the electrical resistance and sheet resistance could be precisely tuned (323−756 Ω and 7−17 Ω $\square^{-1}$, respectively) depending on the number of 3D printed nanofiber layers (40−100 layers). The expected data in Figure 5D are based on calculations according to the measured dimensions (given in Table S3) and the resistivity of 3D printed Ag microstructures reported by An et al.[30] On the basis of the measurements of the resistance and the dimensions of the 3D Ag nanowires, the average resistivity of the transparent electrode was calculated to be 3×10^{-7} Ω m. This value is comparable to those of 3D printed Ag structures prepared by inkjet printing (3×10^{-7} Ω m)[30] and 2D printed Ag ink (2×10^{-7} Ω m).[31] In contrast, the electrodes prepared from 3D stacked nanofibers with 40−100 layers (heights of 3.3 ± 0.3 to 11.5 ± 1.0 μm) showed excellent agreement to the expected values (Figure 5D), whereas the 3D Ag electrode prepared from 20-layer high nanowires (height: ∼ 2.4 ± 0.2 μm) yielded an abnormally high resistance. As we investigated the morphologies of 3D Ag nanowires, unlike the Ag nanowires with higher aspect ratios the 20-layer high Ag nanowires had fluffy and partially damaged edges, as indicated by the yellow arrows in Figure S8. We believe this could be attributed to weak adhesion between the PDMS layer and the 3D Ag nanowire. Nevertheless, this demonstrates the importance of the high aspect ratio of the 3D nanoarchitecture.

It is remarkable that this simple, clean-room-free process can provide such excellent tunability and reproducibility of the electrical resistance of the 3D transparent nanoelectrode. The robust and precise control of the electrical resistance was further validated by comparing the light intensity of light-emitting diodes (LEDs) connected through transparent electrodes with 3D Ag nanowires of different heights, as shown in Figure 5E. When a voltage was applied to the circuit, a distinct gradient of light intensity was observed depending on the height of the Ag nanowire. From the optical and electrical characterizations, it is important to note that this method can potentially avoid the trade-off between transmittance and resistance in transparent electrodes by providing an array of 3D Ag nanowires with high aspect ratios, which impart high conductivity but have little influence on light transmission.

DOI: 10.1021/acs.nanolett.9b04162
Nano Lett. XXXX, XXX, XXX−XXX

A direct comparison between the transparent electrodes with the proposed 3D Ag nanowires with high aspect ratios and the previously reported transparent electrodes based on Ag nanowires/patterns is shown in Figure S9.[32−40] In virtue of the narrow line width (400 nm) and tunable aspect ratio of the 3D nanowalls (up to 48 height/width), it was possible to avoid the trade-off between resistance and transmittance and to achieve improved performance.

In summary, we presented a straightforward and robust NFES method for the rapid fabrication of 3D nanofibrous architectures with high aspect ratios. Compared with other NFES techniques used to build 3D structures, which have been limited to micron-sized structures or special shapes (Table S4), this technique offers a method of nanoprinting 3D structures with precise, self-aligned walls into varied nanoarchitecture designs on demand. The addition of NaCl to the polymer solution increases the electrostatic attraction between the deposited fibers and the nanofiber jet by providing the solution with high conductivity. This strong electrostatic attraction between the aerial jet and the previously deposited fibers was shown to enable effortless self-alignment that facilitates the construction of various nanoskyscraper designs, such as straight and curved nanowalls, nanojungle gyms, and nanobridges, by moving the collecting substrate on an $X-Y$ stage following a predesigned trajectory. The fabricated nanofibrous architectures had widths in the range of 92 ± 3 to 239 ± 30 nm and lengths equal to 2 cm. With a width of 239 ± 30 nm, the height could be controlled from 1.0 ± 0.2 to 11.4 ± 0.9 μm (aspect ratio, 4−48), whereas with a width of 92 ± 3 nm the height was controllable from 0.8 ± 0.1 to 6.6 ± 0.1 μm (aspect ratio, 8−72). By adjusting the number of 3D printed layers, the height of the nanostructure could be tuned precisely. This gave facile control over the electrical resistance of 3D metal nanowires embedded in flexible substrates and yielded high aspect ratios, while avoiding a trade-off with transmittance. Taken together, this facile and precise NFES technique for 3D printing nanofibers possesses tremendous potential for future applications in nanoelectronics, smart materials, and biomedical devices.

■ ASSOCIATED CONTENT

Supporting Information

The Supporting Information is available free of charge at https://pubs.acs.org/doi/10.1021/acs.nanolett.9b04162.

Detailed description of experimental methods, additional figures, and a table (PDF)

Effect of salt concentration on 3D printing of NF (AVI)

Electrostatic attraction between deposited fibers and polymer solution (AVI)

■ AUTHOR INFORMATION

Corresponding Author

*E-mail: ykcho@unist.ac.kr.

ORCID

Hyunhyub Ko: 0000-0003-2111-6101

Yoon-Kyoung Cho: 0000-0001-6423-1834

Present Address

[‖](J.M.O.) Department of Chemical Engineering, Pohang University of Science and Technology, 77 Cheongam-ro, Nam-gu, Pohang 37673, Republic of Korea.

Author Contributions

[⊥]Y.-S.P. and J.K. contributed equally.

Author Contributions

The manuscript was written based on contributions from all authors. All authors have approved the final version of the manuscript.

Notes

The authors declare no competing financial interest.

■ ACKNOWLEDGMENTS

The work was supported by the Institute for Basic Science of Korea (IBS-R020-D1).

■ ABBREVIATIONS

2D, two-dimensional; 3D, three-dimensional; CCD, charge-coupled device; DC, direct current; DI, deionized; EDS, energy-dispersive X-ray spectroscopy; EHD printing, electrohydrodynamic printing; LED, light-emitting diodes; MES, melt electrospinning; NFES, near-field electrospinning; PEO, poly(ethylene oxide); PDMS, polydimethylsiloxane; RPM, revolutions per minute; SEM, scanning electron microscopy; UV−vis, ultraviolet visible.

■ REFERENCES

(1) Xue, J.; Wu, T.; Dai, Y.; Xia, Y. *Chem. Rev.* **2019**, *119* (8), 5298−5415.

(2) Sun, D.; Chang, C.; Li, S.; Lin, L. *Nano Lett.* **2006**, *6* (4), 839−842.

(3) He, X.-X.; Zheng, J.; Yu, G.-F.; You, M.-H.; Yu, M.; Ning, X.; Long, Y.-Z. *J. Phys. Chem. C* **2017**, *121* (16), 8663−8678.

(4) Bisht, G. S.; Canton, G.; Mirsepassi, A.; Kulinsky, L.; Oh, S.; Dunn-Rankin, D.; Madou, M. J. *Nano Lett.* **2011**, *11* (4), 1831−1837.

(5) Liu, Z. H.; Pan, C. T.; Yen, C. K.; Lin, L. W.; Huang, J. C.; Ke, C. A. *Appl. Surf. Sci.* **2015**, *346*, 291−301.

(6) Chang, C.; Tran, V. H.; Wang, J.; Fuh, Y.-K.; Lin, L. *Nano Lett.* **2010**, *10* (2), 726−731.

(7) Fuh, Y.-K.; Ye, J.-C.; Chen, P.-C.; Ho, H.-C.; Huang, Z.-M. *ACS Appl. Mater. Interfaces* **2015**, *7* (31), 16923−16931.

(8) Fuh, Y.-K.; Wu, Y.-C.; He, Z.-Y.; Huang, Z.-M.; Hu, W.-W. *Mater. Sci. Eng., C* **2016**, *62*, 879−887.

(9) Zhang, B.; He, J.; Li, X.; Xu, F.; Li, D. *Nanoscale* **2016**, *8* (34), 15376−15388.

(10) Brown, T. D.; Dalton, P. D.; Hutmacher, D. W. *Adv. Mater.* **2011**, *23* (47), 5651−5657.

(11) He, J.; Xia, P.; Li, D. *Biofabrication* **2016**, *8* (3), 035008.

(12) He, J.; Xu, F.; Dong, R.; Guo, B.; Li, D. *Biofabrication* **2017**, *9* (1), 015007.

(13) Visser, J.; Melchels, F. P. W.; Jeon, J. E.; van Bussel, E. M.; Kimpton, L. S.; Byrne, H. M.; Dhert, W. J. A.; Dalton, P. D.; Hutmacher, D. W.; Malda, J. *Nat. Commun.* **2015**, *6*, 6933.

(14) Wunner, F. M.; Wille, M.-L.; Noonan, T. G.; Bas, O.; Dalton, P. D.; De-Juan-Pardo, E. M.; Hutmacher, D. W. *Adv. Mater.* **2018**, *30* (20), 1706570.

(15) Zeng, J.; Wang, H.; Lin, Y.; Zhang, J.; Liang, F.; Fang, F.; Yang, F.; Wang, P.; Zhu, Z.; Chen, X.; Chen, X.; Wang, Z.; Cai, N.; Tang, Y.; Wu, P. *Microfluid. Nanofluid.* **2018**, *22* (2), 23.

(16) Huang, Y.; Bu, N.; Duan, Y.; Pan, Y.; Liu, H.; Yin, Z.; Xiong, Y. *Nanoscale* **2013**, *5* (24), 12007−12017.

(17) He, J.; Xu, F.; Cao, Y.; Liu, Y.; Li, D. *J. Phys. D: Appl. Phys.* **2016**, *49* (5), 055504.

(18) Lee, M.; Kim, H.-Y. *Langmuir* **2014**, *30* (5), 1210−1214.

(19) Kim, H.-Y.; Lee, M.; Park, K. J.; Kim, S.; Mahadevan, L. *Nano Lett.* **2010**, *10* (6), 2138−2140.

(20) Zhao, S.; Zhou, Q.; Long, Y.-Z.; Sun, G.-H.; Zhang, Y. *Nanoscale* **2013**, *5* (11), 4993−5000.

DOI: 10.1021/acs.nanolett.9b04162
Nano Lett. XXXX, XXX, XXX−XXX

(21) Choi, W.; Kim, G. H.; Shin, J. H.; Lim, G.; An, T. *Nanoscale Res. Lett.* **2017**, *12* (1), 610.
(22) Kim, G. H.; Nam, H.; Choi, W.; An, T.; Lim, G. *Adv. Mater. Interfaces* **2018**, *5* (5), 1701204.
(23) Park, S. M.; Kim, D. S. *Adv. Mater.* **2015**, *27* (10), 1682−1687.
(24) Luo, G.; Teh, K. S.; Liu, Y.; Zang, X.; Wen, Z.; Lin, L. *ACS Appl. Mater. Interfaces* **2015**, *7* (50), 27765−27770.
(25) Collins, G.; Federici, J.; Imura, Y.; Catalani, L. H. *J. Appl. Phys.* **2012**, *111* (4), 044701.
(26) Sun, B.; Long, Y.-Z.; Yu, F.; Li, M.-M.; Zhang, H.-D.; Li, W.-J.; Xu, T.-X. *Nanoscale* **2012**, *4* (6), 2134−2137.
(27) Vong, M.; Speirs, E.; Klomkliang, C.; Akinwumi, I.; Nuansing, W.; Radacsi, N. *RSC Adv.* **2018**, *8* (28), 15501−15512.
(28) Reis, T. C.; Correia, I. J.; Aguiar-Ricardo, A. *Nanoscale* **2013**, *5* (16), 7528−7536.
(29) Ahirwal, D.; Hébraud, A.; Kádár, R.; Wilhelm, M.; Schlatter, G. *Soft Matter* **2013**, *9* (11), 3164−3172.
(30) An, B. W.; Kim, K.; Lee, H.; Kim, S.-Y.; Shim, Y.; Lee, D.-Y.; Song, J. Y.; Park, J.-U. *Adv. Mater.* **2015**, *27* (29), 4322−4328.
(31) Yoon, J.-W.; Noh, B.-I.; Jung, S.-B. *Microelectron. Reliab.* **2014**, *54* (2), 410−416.
(32) Kang, M. G.; Kim, M. S.; Kim, J.; Guo, L. J. *Adv. Mater.* **2008**, *20* (23), 4408−4413.
(33) De, S.; Higgins, T. M.; Lyons, P. E.; Doherty, E. M.; Nirmalraj, P. N.; Blau, W. J.; Boland, J. J.; Coleman, J. N. *ACS Nano* **2009**, *3* (7), 1767−1774.
(34) Jiu, J.; Nogi, M.; Sugahara, T.; Tokuno, T.; Araki, T.; Komoda, N.; Suganuma, K.; Uchida, H.; Shinozaki, K. *J. Mater. Chem.* **2012**, *22* (44), 23561−23567.
(35) van de Groep, J.; Spinelli, P.; Polman, A. *Nano Lett.* **2012**, *12* (6), 3138−3144.
(36) Hong, S.; Yeo, J.; Kim, G.; Kim, D.; Lee, H.; Kwon, J.; Lee, H.; Lee, P.; Ko, S. H. *ACS Nano* **2013**, *7* (6), 5024−5031.
(37) Park, J.; Hwang, J. *J. Phys. D: Appl. Phys.* **2014**, *47* (40), 405102.
(38) Schneider, J.; Rohner, P.; Thureja, D.; Schmid, M.; Galliker, P.; Poulikakos, D. *Adv. Funct. Mater.* **2016**, *26* (6), 833−840.
(39) Jang, Y.-R.; Chung, W.-H.; Hwang, Y.-T.; Hwang, H.-J.; Kim, S.-H.; Kim, H.-S. *ACS Appl. Mater. Interfaces* **2018**, *10* (28), 24099−24107.
(40) Jiang, Z.; Fukuda, K.; Xu, X.; Park, S.; Inoue, D.; Jin, H.; Saito, M.; Osaka, I.; Takimiya, K.; Someya, T. *Adv. Mater.* **2018**, *30* (26), 1707526.

DOI: 10.1021/acs.nanolett.9b04162
Nano Lett. XXXX, XXX, XXX−XXX